Direct and Indirect Pathways in Strong Field Atomic Ionization Dynamics

Armelle de Bohan,[1] Bernard Piraux,[1] Lino Ponce,[2] Richard Taïeb,[2] Valérie Véniard,[2] and Alfred Maquet[2]
[1]*Laboratoire de Physique Atomique et Moléculaire, Université catholique de Louvain, Chemin du cyclotron, 2, 1348 Louvain-la-Neuve, Belgium*
[2]*Laboratoire de Chimie Physique-Matière et Rayonnement, Université Pierre et Marie Curie, 11, Rue Pierre et Marie Curie, 75231 Paris Cedex 05, France*
(Received 7 January 2002; published 26 August 2002)

With the help of a suitably chosen momentum-space analysis, we study some of the basic mechanisms governing the physics of the processes occurring when atoms are submitted to intense infrared laser pulses, with peak intensities 10^{14} W cm^{-2} $\leq I_{\max} \leq 10^{15}$ W cm^{-2}. This intensity range is especially interesting because two highly nonlinear atomic processes, namely, above threshold ionization and high-order harmonic generation, take place with significant probabilities. Several issues regarding the dynamics of these processes are resolved, with special attention devoted to the mechanism leading to the ejection of the photoelectrons in this intensity range.

DOI: 10.1103/PhysRevLett.89.113002 PACS numbers: 32.80.Rm, 42.50.Vk

The recent advent of powerful infrared laser sources, routinely delivering femtosecond pulses with peak intensities in the range $10^{14} \leq I_L \leq 10^{15}$ W cm^{-2}, with repetition rates in the kHz regime, has permitted one to produce data with unprecedented precision on above threshold ionization (ATI) and high-order harmonic generation (HHG). These two processes dominate laser-matter physics in this range of intensities. They are interesting because they represent a unique source of information not only about the nonlinear response of atomic systems to intense pulses of radiation, but also from the point of view of applications [1]. At higher intensities, multiple ionization washes out ATI spectra, and HHG propagation in the medium is hampered. In short, this intensity range offers an ideal window for observing interesting, highly nonlinear, atom-laser physics.

At such laser intensities, there is no clear-cut separation between the perturbative regime, where multiphoton processes dominate, and the strong field limit where tunnel ionization is assumed to set in. In fact, there is a subtle interplay between the two mechanisms, as indicated by the fact that the so-called "Keldysh parameter" $\gamma = \frac{\omega}{E}\sqrt{2I_p}$ takes values close to unity [2]. Here ω is the laser field frequency with amplitude E and I_p is the ionization potential of the atom (unless indicated, we use atomic units throughout this paper). Nowadays, one can reproduce delicate resonant features present in ATI spectra with astonishing precision by solving the time-dependent Schrödinger equation (TDSE) for model atomic potentials [3]. However, no simple picture can be drawn for the *mechanism leading to electron ejection* since both theoretically and experimentally the relevant information is extracted after the laser turnoff.

When tunneling ionization ($\gamma \ll 1$) is dominant, photoelectron wave packets are ejected when the field strength is close to its maximum during a laser cycle. This overall behavior contrasts with the perturbative regime ($\gamma \gtrsim 1$), when (time-independent) multiphoton ionization rates can be defined within a good approximation. Thus, a time-dependent approach is compulsory in order to gain insight on physical mechanisms at work in pulsed fields. In this respect, the Keldysh theory [2] and its modern avatar, the so-called "strong field approximation" (SFA) [4], are not directly applicable since they are quasistatic approximations. Moreover, the model relies on the assumptions that the dynamics are governed by the coupling of the ground state with the continuum and that ejected electrons are described by Volkov states that ignore the presence of the Coulomb potential. Such a simplified picture accounts for the high energy features in ATI and HHG spectra and has provided a nontrivial example of the application of Feynman's path integral formalism [5]. However, several theoretical studies [6,7] indicate that ionization yields evaluated in the context of the SFA, by using tunneling rates [8], do not coincide with exact numerical calculations either qualitatively or quantitatively. This is notably the case for the low energy part of the ATI spectra, up to $2U_p$ [9], which contains the dominant part of the ionization current. These discrepancies have motivated numerous contributions dedicated to the introduction of Coulomb corrections in the SFA theory [8,10–12] and comparisons to experiments have been made [13]. In addition, recent improvements have been reported concerning nonadiabatic corrections in order to define time-dependent ionization rates in the context of double ionization; see [14].

The main motivation of the present analysis is to reconsider the mechanism leading to ionization within this energy range and to elucidate the role of the Coulomb potential. To this end, we study the time evolution of the wave function by solving numerically the TDSE for atomic hydrogen *in momentum space* [15]. This approach is numerically attractive because the global probability density remains localized in this space. We have adopted the velocity form of the laser-atom interaction [16]. Then, the canonical momentum $\mathbf{p}(t)$, which is conserved for a free electron, does not coincide with the velocity (in a.u.), $\mathbf{v}(t)$:

$$\mathbf{p}(t) = \mathbf{v}(t) - \mathbf{A}(t), \tag{1}$$

where $\mathbf{A}(t) = A(t)\hat{\mathbf{z}}$ is the vector potential associated with the linearly polarized laser field. This momentum analysis is well suited to probe the dynamics and the atomic potential effects—in our case the Coulomb potential—as shown by Ehrenfest's theorem with respect to the canonical momentum:

$$\left\langle \frac{d\mathbf{p}}{dt} \right\rangle = -\langle \boldsymbol{\nabla} V \rangle. \tag{2}$$

Before investigating closer the potential issue, we first illustrate the consequences of these fundamental relations by means of Fig. 1, where the time evolution of the component of the probability density along p_z is shown. The transverse component p_n is set equal to zero. The main features of this time evolution can be understood thanks to Eqs. (1) and (2). Part of the probability density experiences an oscillatory motion, while conspicuous "stripes" corresponding to constant values of p_z emerge after two laser cycles. The oscillating fraction of the probability density can be associated with the bound part of the population as the average velocity along the z axis reads

$$\langle v_z(t) \rangle_{\text{bound}} \approx 0 \Leftrightarrow \langle p_z(t) \rangle_{\text{bound}} \approx -A(t), \tag{3}$$

in agreement with the observed oscillations in phase opposition with $A(t)$. On the other hand, the stripes represent ionizing wave packets starting to be ejected after the second laser period and being reinforced after each cycle. Applying Ehrenfest's theorem to an ionizing wave packet gives

$$\left\langle \frac{dp_z}{dt} \right\rangle_{\text{ion}} = -\langle \nabla_z V \rangle_{\text{ion}} \approx 0. \tag{4}$$

As expected, each stripe can be associated with a peak in the ATI spectrum. Its structures appear after the second laser cycle when a second wave packet, with the same canonical momentum, emerges in the same direction. From this time dependence of the probability density, it appears that ATI structures result from quantum interferences between wave packets ejected every laser cycle [17]. Furthermore, a closer inspection of Fig. 1 reveals that, within half a cycle, stripes emerge sequentially at times t_{ion} with mean canonical momenta along z given by

$$p_z^{\text{ion}} \approx -A(t_{\text{ion}}). \tag{5}$$

This means that wave packets are indeed ejected with a null velocity along z; they emerge directly from the bound state as it moves along p_z like $-A(t)$, in good agreement with the SFA. However, at this laser intensity, the Keldysh parameter is $\gamma = 0.75$, a value which suggests that multiphoton absorption should remain important. As shown next, our momentum-space approach helps to define more precisely the transition between the two regimes. Within the framework of the SFA, one can relate the time dependence of $\langle v_z(t) \rangle$ to the one of the vector potential $\mathbf{A}(t)$ and consequently to the population density transferred into the continuum. This comes from the assumption that the wave function of the system reduces to the superposition of the *unperturbed* ground state and of a wave packet in the continuum:

$$|\psi(t)\rangle \approx a_{1s}(t)|\phi_{1s}\rangle + \int d\mathbf{k}\, g(\mathbf{k}, t)|\phi_{\mathbf{k}}\rangle, \tag{6}$$

This entails that one has approximately [15]

$$\langle v_z(t) \rangle \approx A(t) \int d\mathbf{k} |g(\mathbf{k}, t)|^2, \tag{7}$$

where $\int d\mathbf{k}|g(\mathbf{k}, t)|^2$ is the fraction of the population in the continuum. In the tunneling regime, the latter increases by steps at each half period, when the field strength is close to its maximum, i.e., when a burst of photoelectrons is ejected. On the contrary, in the multiphoton regime, the atom can be ionized at any time during the cycle. The difference between the two regimes is clearly identified in Figs. 2. At $I = 10^{14}$ W cm^{-2}, i.e., for $\gamma = 1.07$, ionization yields are already significant. However, as shown in Fig. 2(a), no phase relation exists between $\langle v_z(t) \rangle$ and $A(t)$, revealing the dominance of multiphoton absorption. On the contrary, already at $I = 2 \times 10^{14}$ W cm^{-2}, i.e., for $\gamma = 0.75$, there is a clear linear dependence of $\langle v_z(t) \rangle$ on $A(t)$ [see Fig. 2(b)]. One notes also that the slope increases by steps at each half-cycle, in global agreement with Eq. (7) from the SFA picture. Therefore, we suggest that the phase relation between $\langle v_z(t) \rangle$ and $A(t)$ defines another criterion to discriminate between the multiphoton and the strong field regime. This criterion is less restrictive than Keldysh's

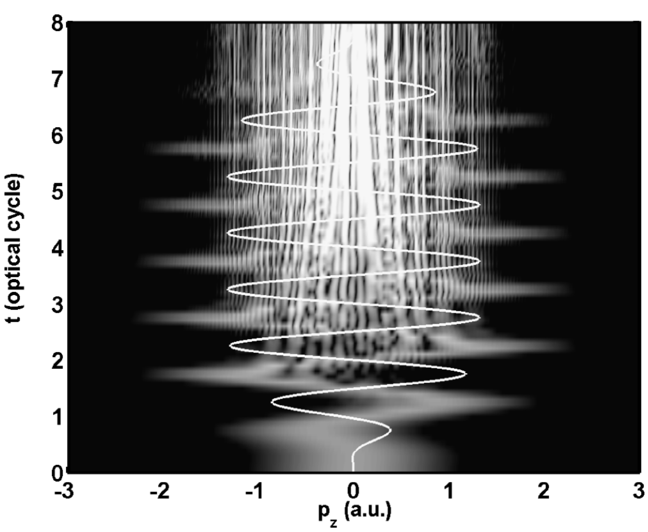

FIG. 1. Electron probability density as a function of time and p_z, for the interaction of H with an eight-cycle pulse with $I_0 = 2 \times 10^{14}$ W cm^{-2} and $\omega = 0.057$ a.u. $p_n = 0$ and the solid line represents $A(t)$.

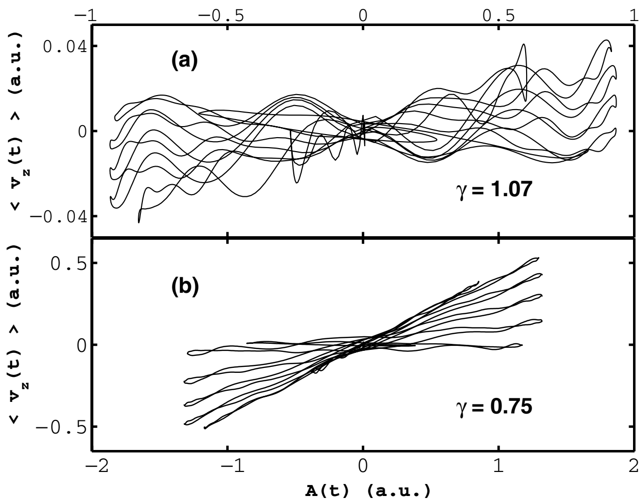

FIG. 2. Average instantaneous velocity along **z** as a function of $A(t)$ (same pulse shape as in Fig. 1). (a) $I = 10^{14}\ \mathrm{W\,cm^{-2}}$; (b) $I = 2 \times 10^{14}\ \mathrm{W\,cm^{-2}}$.

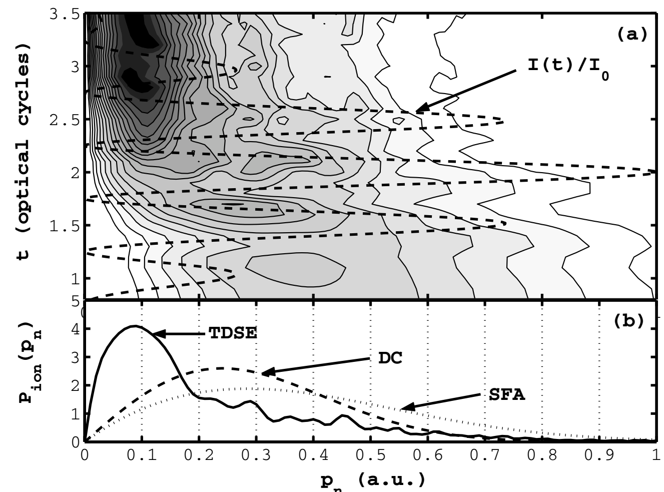

FIG. 3. (a) $P(p_n, t)$ as defined by Eq. (8) for a sine square laser pulse of full duration $\Delta t = 4T$ (optical cycle), $I_0 = 5 \times 10^{14}\ \mathrm{W\,cm^{-2}}$, $\omega = 0.057$ a.u. Dashed line is the normalized instantaneous intensity. (b) $P_{\mathrm{ion}}(p_n)$ extracted from our TDSE results, $P_{\mathrm{ion}}^{\mathrm{SFA}}(p_n)$ [see Eq. (9)] and the dc tunneling prediction; see [18].

$\gamma \ll 1$ since the strong field dynamics is clearly evidenced at intensities such as when γ is still close to unity.

At higher intensities, we are able to probe the effect of the Coulomb potential in the ejection mechanism [8,10–12]. This effect can be evidenced by considering the momentum distribution in the transverse direction $\mathbf{p_n}$. To this end, we define the reduced probability density:

$$P(p_n, t) = 2\pi\, p_n \int_{-\infty}^{+\infty} dp_z |\psi(p_z, p_n, t)|^2. \qquad (8)$$

In Fig. 3(a), we show a contour plot of $P(p_n, t)$ for a four-cycle pulse with peak intensity $5 \times 10^{14}\ \mathrm{W\,cm^{-2}}$ ($\gamma = 0.48$). Ionization is significant (70%) and occurs essentially between the first and the third optical cycles. In Fig. 3(b), we compare the ionized fraction of the probability density $P_{\mathrm{ion}}(p_n)$ obtained from our TDSE calculations (at the end of the interaction), the SFA equivalent which has an overall behavior given by

$$P_{\mathrm{ion}}^{\mathrm{SFA}}(p_n) \propto p_n \int dp_z |d_{1s}(p_z, p_n)|^2, \qquad (9)$$

where $d_{1s}(\mathbf{p})$ is the bound-free dipole matrix element and the dc tunneling prediction given in [18]. One observes a clear deviation between SFA together with the dc tunneling case and TDSE. Indeed, not only the SFA and dc distributions are wider but also they both exhibit a maximum at $p_n \approx 0.25$–0.3 a.u., while our result predicts a dominant ionization peak located at $p_n = p_{n0} = 0.1$ a.u. Results obtained by means of classical trajectory Monte Carlo simulations also exhibit this shifted dominant peak [19]. Moreover, we can trace its birth thanks to Fig. 3(a). Each half optical cycle, at peak field, a wave packet is created and its maximum location agrees with SFA. But then, within the same half-cycle, as the field decreases, this wave packet shifts towards p_{n0}. The presence of this transverse momentum transfer, favoring ejection along the polarization axis, highlights the "*focusing role*" of the Coulomb potential in this mechanism.

In position space, this momentum change can be experienced by ionizing wave packets located close to the *inner side* of the saddle associated with the Coulomb barrier [20]. In addition, it takes place roughly over half a cycle while the barrier of the effective potential tips up. It implies that these wave packets, created after the field gets maximum, remain in the vicinity of the nucleus before their final ejection half a cycle later. We label them "indirect" wave packets in contrast to the "direct" ones that never reencounter the ion core and that are ejected before the field reaches the maximum of its strength.

One can discriminate between "direct" and "indirect" wave packet contributions to ionization by considering the quantity

$$F_{12}(t) = 2\pi \int_{p_{z_1}}^{p_{z_2}} dp_z \int_0^{\infty} dp_n p_n |\psi(p_z, p_n, t)|^2, \qquad (10)$$

which represents the fraction of the probability density contained at t, within an interval $\Delta p_{z_{1,2}} = [p_{z_1}, p_{z_2}]$. The time variations of $F_{12}(t)$, shown in Fig. 4(b), consist of almost flat parts separated by peaks located at each half-cycle. Within a given interval $\Delta p_{z_{1,2}}$, the latter arise when the ground state probability density, which oscillates as $-A(t)$ (see Eq. (3) and Fig. 1), "crosses" $\Delta p_{z_{1,2}}$, leading to an ionizing wave packet with typical momentum given by Eq. (5). Therefore, the stepwise increase of the flat part of $F_{12}(t)$ around a peak corresponds to the growth of the ionizing fraction in $\Delta p_{z_{1,2}}$. Because of the sign reversal of $A(t)$, "indirect" and "direct" wave packets are associated with a

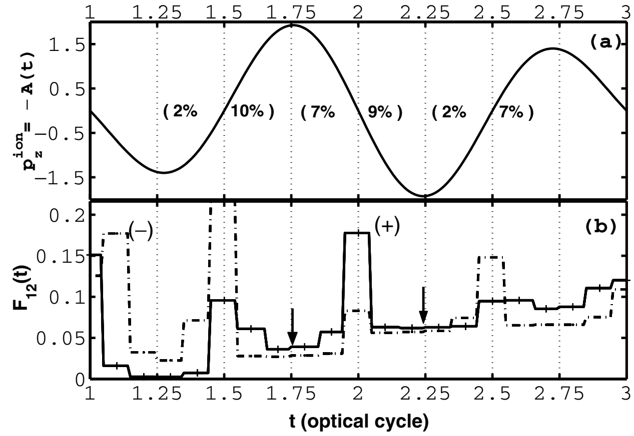

FIG. 4. (a) $p_z^{\rm ion} = -A(t_{\rm ion})$ [see Eq. (5) and text]. (b) $F_{12}^{(+)/(-)}(t)$ [see Eq. (10)] for two symmetric intervals $0.25 < |p_z| < 0.5$ a.u. [same field parameters as in Fig. 3(a)]. In (a), between brackets, ionization fractions due to (direct, indirect) calculated on a wider interval $|p_z| < 1$ a.u. It reveals that $26/37 \approx 70\%$ comes from an indirect process and $11/37 \approx 30\%$ from a direct one.

unique direction (either positive or negative p_z) within time intervals delimited by subsequent extrema of $A(t)$, i.e., around one extremum of $E(t)$ [see Fig. 4(a)]. For example, in the central time interval $[1.75T, 2.25T]$, wave packets with positive canonical momentum will be direct since they are emitted *before* peak field, while wave packets with negative canonical momentum will be indirect since they are emitted *after* peak field. Around $t = 2T$, when $A(t) = 0$, we see that the increase of $F_{12}^{(-)}$ [indirect, see arrows in Fig. 4(a)] is higher than the corresponding increase of $F_{12}^{(+)}$ (direct). Over a range of momenta such that $|p_z| < 1$ a.u., the same analysis shows that "indirect" wave packets are dominant with respect to "direct" (70% versus 30%) contributions. This contrasts markedly with the predictions of the SFA model, where one cannot distinguish between these contributions, *since tunneling rates depend only on the field amplitude.*

In conclusion, the above presented momentum-space analysis helps to uncover the actual mechanisms contributing to the dominant part of ATI spectra, up to $2U_p$. At intensities such that the Keldysh parameter γ is close to unity, it is possible to identify two distinct ionization mechanisms termed "direct" and "indirect." A remarkable asymmetry, favorable to "indirect" wave packets, is physically consistent with the momentum changes observed in Figs. 1 and 3. It represents an unambiguous signature of the determinant role of the Coulomb potential. This contrasts with the situation at higher ejection energies where the role of the Coulomb potential is less significant. Another advantage of the momentum-space analysis is to provide a convenient tool for exploring the transition between the multiphoton and the strong field regimes. These promising features should serve as an incentive for developing new computational tools adapted to such momentum-space approaches.

The Laboratoire de Chimie Physique-Matière et Rayonnement is UMR 7614 du CNRS, and is LRC No. DSM-98-16 with the CEA. A. M. thanks the U.C.L. for a one month visit. We are grateful to A. Scrinzi for stimulating discussions.

[1] Recent reviews are P. Salières *et al.*, Adv. At. Mol. Opt. Phys. **41**, 83 (1999), and Th. Brabec and F. Krausz, Rev. Mod. Phys. **72**, 545 (2000).
[2] L. V. Keldysh, Zh. Eksp. Teor. Fiz. **47**, 1945 (1964); Sov. Phys. JETP **20**, 1307 (1965).
[3] M. J. Nandor *et al.*, Phys. Rev. A **60**, R1771 (1999).
[4] M. Lewenstein *et al.*, Phys. Rev. A **49**, 2117 (1994); M. Lewenstein *et al.*, Phys. Rev. A **51**, 1495 (1995). Earlier references are F. H. M. Faisal, J. Phys. B **6**, L89 (1973); H. R. Reiss, Phys. Rev. A **22**, 1786 (1980).
[5] P. Salières *et al.*, Science **292**, 902 (2001).
[6] D. Bauer and P. Mulser, Phys. Rev. A **59**, 569 (1999).
[7] A. Scrinzi *et al.*, Phys. Rev. Lett. **83**, 706 (1999).
[8] M. V. Ammosov *et al.*, Sov. Phys. JETP **64**, 1191 (1986).
[9] Here $U_p = F^2/(4\omega^2)$ is the ponderomotive energy acquired by the electron within the field.
[10] A. M. Perelomov *et al.*, Sov. Phys. JETP **23**, 924 (1966).
[11] A. M. Perelomov and V. S. Popov, Sov. Phys. JETP **25**, 336 (1967).
[12] A recent discussion can be found in G. L. Yudin and M. Yu. Ivanov, Phys. Rev. A **63**, 033404 (2001).
[13] F. A. Ilkov *et al.*, J. Phys. B **25**, 4005 (1992).
[14] G. L. Yudin and M. Y. Ivanov, Phys. Rev. A **64**, 013409 (2001).
[15] Details can be found in A. de Bohan, "Thèse de Doctorat," Université catholique de Louvain, 2001.
[16] E. Cormier and P. Lambropoulos, J. Phys. B **29**, 1667 (1996).
[17] A similar effect for harmonic generation has been discussed in J. B. Watson *et al.*, Phys. Rev. A **55**, 1224 (1997).
[18] N. B. Delone *et al.*, Laser Phys. **3**, 312 (1993).
[19] L. Ponce *et al.* (unpublished).
[20] R. Shakeshaft *et al.*, Phys. Rev. A **42**, 1656 (1990).